JOURNAL OF GEOPHYSICAL RESEARCH, VOL. 101, NO. D18, PAGES 23,311–23,316, OCTOBER 27, 1996

The influence of inclusions on light scattering by large ice particles

Andreas Macke
Department of Applied Physics, Columbia University, New York
NASA Goddard Institute for Space Studies, New York

Michael I. Mishchenko
NASA Goddard Institute for Space Studies, New York
Institute of Terrestrial and Planetary Atmospheres, State University of New York at Stony Brook

Brian Cairns
Department of Applied Physics, Columbia University, New York
NASA Goddard Institute for Space Studies, New York

Abstract. The scattering of visible light by ice crystals containing scattering and absorbing inclusions is calculated by a combination of ray-tracing and Monte Carlo techniques. Results are shown for a randomly oriented hexagonal ice column containing ammonium sulfate particles, soot particles, and air bubbles. It is shown that a noticeable change in the ice crystal scattering properties compared to a pure crystal requires about 10^3 to 10^4 internal scatterers of a size comparable to the wavelength. While the nonabsorbing ammonium and air bubble inclusions generally decrease the asymmetry parameter g , soot provides a strong increase in g caused by the additional absorption. An independent superposition of the scattering properties of ice crystal and inclusions does not give satisfactory results because of the strong influence of internal scatterers on the characteristic ray paths inside the crystal. Multiple-scattering calculations show that the strongest changes in the radiative fluxes are associated with the soot contaminated ice crystals.

1. Introduction

The study of light scattering by atmospheric ice crystals is basically motivated by the large variability of ice particle shapes [*Macke,* 1993; *Takano and Liou,* 1995; *Macke et al.,* 1996]. In these studies, the ice material itself is assumed to be free of any impurities. In fact, while the shape problem is obvious from numerous in situ aircraft measurements [e.g., *Heymsfield et al.,* 1990], little is known about the internal structure of the ice particles. With regard to a possible increase of the concentration of aerosol particles in the upper troposphere, either due to natural phenomena like volcanic eruptions [*Sassen et al.,* 1995] or due to anthropogenic causes like high-altitude aircraft exhausts [*Schumann,* 1994] or high-reaching convective transport of industrial combustions [*Raes et al.,* 1995], increased scavenging and aggregation processes may well lead to a large number of trapped particles inside an ice crystal. According to *Jensen and Toon* [1994], an indirect aerosol effect, i.e., a change in the ice particle size distribution due to an increased aerosol number density, is rather unlikely.

Contrary to water droplets, soluble particles trapped inside an ice crystal may not go into solution. Thus these particle will not change the overall refractive index of the crystal but act as internal scatterers. If their sizes are comparable to the wavelength of the incoming radiation, resonance phenomena may result in large extinction efficiencies of these scatterers, which, in turn, may strongly increase their radiative effects.

The purpose of this study is to demonstrate the potential effects of these internal scatterers on the ice crystal single- and multiple-scattering properties. Single-scattering calculations are performed by combining ray-tracing and Monte Carlo techniques, as well as by an independent superposition of the individual scattering properties of ice crystal and inclusions. Multiple scattering is treated in the Monte Carlo approximation. Results are shown for the following three different types of inclusions: ammonium sulfate, air bubbles and soot.

2. Ray-Tracing/Monte Carlo Model

The scattering of a light ray entering a particle containing distinct scattering inclusions is simulated by a combination of ray tracing (RT) and Monte Carlo

Paper number 96JD02364.
0148-0227/96/96JD-02364$09.00

(MC) techniques. While the ray tracing program takes care of the individual reflection and refraction events at the outer boundary of the particle, the Monte Carlo routine simulates internal scattering processes. Detailed descriptions of the ray tracing model are given by *Macke* [1993] and *Macke et al.* [1996].

After an incident photon is refracted into the crystal, it travels a free path length l given by

$$l = - < l > \log[R(0,1)], \quad (1)$$

where $< l >$ is the mean free path length between two subsequent scattering events and $R(0,1)$ is an equally distributed random number within the interval $(0,1)$.

If the photon has not reached one of the boundaries of the medium, its previous direction is changed along the local zenith θ and azimuth ϕ scattering angles according to

$$\int_0^{\theta} P^{(i)}(\theta) \sin\theta d\theta = R(0,1) \int_0^{\pi} P^{(i)}(\theta) \sin\theta d\theta \quad (2)$$

$$\phi = R(0, 2\pi), \quad (3)$$

where $P^{(i)}(\theta)$ denotes the scattering phase function of the internal scatterer. Absorption is taken into account by multiplying the photon energy with the single scattering albedo $\omega_0^{(i)}$ of the internal scatterers.

The processes stated in (1) and (2) are repeated until the photon enters one of the crystal facets, where it is again subject to reflection and refraction events. The whole procedure is again repeated for the internally reflected component until the photon energy falls below 10^{-5} times the incident energy.

The angular dependency of the overall scattered energy is described by a scattering phase function

$$P(\theta) = \frac{1}{2\omega_0}[(2\omega_0 - 1)P_{\mathrm{ref}}(\theta) + P_{\mathrm{dif}}(\theta)], \quad (4)$$

where $P_{\mathrm{ref}}(\theta)$ denotes the phase function due to the reflection/refraction and internal scattering events and $P_{\mathrm{dif}}(\theta)$ takes diffraction at the ice crystals projected area into account. Here ω_0 denotes the total single-scattering albedo of the ice particle. Note that ω_0 is always larger than 0.5 in the geometric optics approximation since half of the incident light is always diffracted.

The anisotropy of the scattered radiation is described by the asymmetry parameter

$$g = < \cos\theta > = \int_0^{\pi} P(\theta) \cos\theta \sin\theta d\theta \quad (5)$$

Note that the incorporation of RT and MC techniques contains the following two assumptions. First, the distance between the nearest neighbor internal scatterers must be larger than a few times their radius in order to treat them as independent scatterers. Second, the distance between the crystal boundary and internal scatterers also must exceed a certain value in order to assure the validity of the Snellius law and Fresnels formulas. Following the work by *Mishchenko et al.* [1995], we assume that both conditions require a mean free path length larger than 4 times the particles' radii. The random nature of the Monte Carlo process will lead to occasional violations of this requirement. However, by setting the minimum $< l >$ to 20 times the particles radii', we ensure that possible "near-field" interactions play only a minor role in the total scattering simulations.

3. Input Data

The effects of internal impurities are studied for one hexagonal-shaped ice column, defined by a length to (hexagonal) diameter ratio of 200 μm/100 μm. This geometry corresponds to a mean particle size as observed in natural cirrus clouds.

The following types of internal scatterers are considered here: ammonium sulfate aerosols ($(NH_4)_2SO_4$), soot particles, and air bubbles. Ammonium sulfate and soot particles are naturally occurring aerosol types. Air bubbles may be trapped inside rapidly growing ice particles or inside suddenly frozen supercooled water droplets (J. Hallet, private communication, 1995). The choice of these types of internal scatterers was also motivated by the fact that they represent different kinds of optical properties (see Figure 1). Both ammonium sulfate and air bubbles are transparent in the visible. However, air bubbles scatter light more isotropically than ammonium sulfate particles do. Therefore these particles only affect the anisotropy of the ice crystals' scattering phase function. Soot, on the other hand, is strongly absorbing and therefore has the potential of increasing the ice particle absorption. We assume that the sizes of these impurities obey a standard gamma distribution defined by an effective radius r_{eff} and an effective variance ν_{eff} [*Hansen and Travis,* 1974]. The values chosen for the three scatterers are given in Table 1. The refractive indices $n = n_r + in_i$ are taken from *Toon et al.* [1976] for $(NH_4)_2SO_4$, and from *Nils-*

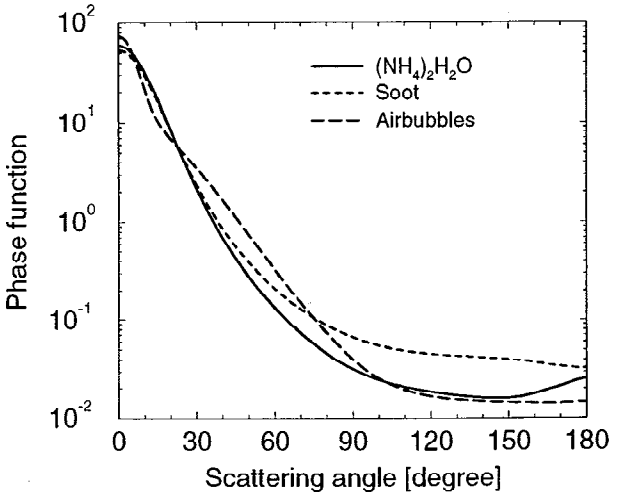

Figure 1. Scattering phase functions of spherical inclusions made of ammonium sulfate, soot, and air bubbles.

Table 1. Variable Values for the Three Types of Inclusions

Type	r_{eff}, μm	ν_{eff}	n_r, n_i
$(NH_4)_2SO_4$	0.5	0.2	1.15, 0.0
Soot	0.5	0.2	1.18, 0.38
Air bubbles	1.0	0.1	0.75, 0.0
Type	Q_{ext}	ω_0	g
$(NH_4)_2SO_4$	1.354	1.0000	0.9213
soot	2.122	0.4257	0.9033
air bubbles	1.977	1.0000	0.8817

Here r_{eff} is effective radius; ν_{eff} is effective variance; (n_r, n_i) are their relative refractive indices; Q_{ext} is resulting averaged extinction efficiency; ω_0 is single-scattering albedo; and g is asymmetry parameter.

son [1979] for soot. For air bubbles we assume that $n = 1.0$. These values are divided by the refractive index of ice [*Warren,* 1984], where the small imaginary part ($\sim 10^{-9}$) is neglected to obtain the relative refractive indices (see Table 1). Since spherical particle shapes were assumed, Mie theory was used to obtain the size distributional averaged optical properties of the internal scatterers relative to the surrounding ice material. Note that this procedure requires that the surrounding ice is nonabsorbing, which limits our study to visible wavelengths.

Our calculations were performed at a wavelength of $\lambda = 0.55$ μm, i.e., at the maximum of the solar irradiation. The resulting extinction efficiencies Q_{ext}, single-scattering albedos ω_0, and asymmetry parameters are shown in Table 1. Figure 1 compares the phase functions of the internal scatterers.

The density of the inclusions is described by the mean free path length $< l >$ (see (1)), or, equivalently, by the volume extinction coefficient $\beta_x = 1/ < l >$. For an ensemble of N particles per volume element whose sizes obey a standard gamma distribution, β_x is given by (Lacis and Mishchenko 1995)

$$\beta_x = \pi r_{\text{eff}}^2 (1 - \nu_{\text{eff}})(1 - 2\nu_{\text{eff}}) Q_{\text{ext}} N, \qquad (6)$$

where r_{eff} and ν_{eff} denote effective radius and effective variance , respectively, of the size distribution.

For the purpose of interpretation, it is convenient to compare a given mean free path length to a characteristic crystal dimension H. In the case of clouds, H is given by the cloud vertical dimension, i.e., the geometrical cloud height, and $H/l = \tau$ denotes the cloud optical depth. For randomly oriented finite crystals, where the photons are subject to reflection and transmission events at the outer boundaries, a characteristic length may be defined by the sum over all ray paths l_i, weighted by the fraction of the original incident energy e_i, which is transported along that path, i.e., $H = \sum_{i=1}^{\infty} e_i \cdot l_i$. Note that $e_1 < 1$ since part of the incident energy is already lost due to external reflections. On the other hand, total internal reflections ($e_{i+1} = e_i$) may strongly increase the effective path length. For the ice column used in this paper we find $H \sim 80$ μm. This value is about 1.7 times larger than the so-called "effective distance" [e.g., *Mitchell and Arnott,* 1994], which is defined by the ratio of particle volume to its projected area and which is often used as a characteristic length for single-scattering approximations. Interestingly, we found almost the same factor for quite different crystal shapes like columns, plates, and cubes!

4. Results

4.1. Single-Scattering Simulations With the ray-tracing/Monte Carlo model

Figure 2 demonstrates the effects of internal impurities on the total scattering phase function. Results are shown for mean free path lengths $< l > = 400$, 80, and 40 μm, i.e., five times, once, and half the effective distance H. This implies that the average number of internal scattering events along H per incoming light rays is 1/5, 1, and 2, respectively. With decreasing $< l >$, all three inclusions provide a noticeable broadening of the forward scattering features from 0° to 22° , as well as a decrease in the magnitude of the 22° halo maximum. The broadening results from the predominant forward scattering features of the individual impurities, which spread those light rays which are directly transmitted through plane-parallel crystal facets. The same mechanism reduces the intensities of the halos and the backscattering maximum at about 150° , as well as the magnitude of direct backscattering.

The nonabsorbing inclusions provide an increase in side scattering, whereas side scattering decreases in magnitude for those ice crystals which contain soot particles. Both absorbing and nonabsorbing inclusions add more and more forward and side scattering to the

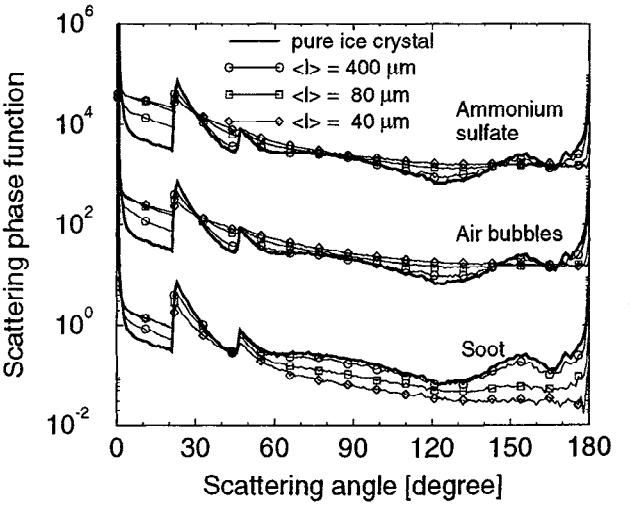

Figure 2. Scattering phase functions of a hexagonal column with internal ammonium sulfate (multiplied by 10^4), air bubbles (multiplied by 10^2), and soot inclusions. The mean free path length for these internal scatterers is $l = 400$, 80, and 40 μm, respectively.

overall scattering features as their number density increases. However, the additional absorption due to the nonconservative scattering at the soot particles reduces the contribution of reflected/refracted rays to the total phase function (see (4)), which explains the opposite side-scattering effect for the ice particles with absorbing and nonabsorbing contaminations.

Note that these deviations from the scattering properties of a pure ice particle are qualitatively different from those resulting from random crystal distortions as discussed by *Macke et al.* [1996]. There, the side-scattering properties between about 60° and 120° scattering angles remain essentially unaffected by the crystal distortions. This is because this regime is basically affected by external reflections, which show only little sensitivity to particle shape. Internal scatterers, on the other hand, can deviate transmitted light rays toward side-scattering angles as demonstrated for the purely scattering ammonium sulfate and air bubble inclusions.

From Figure 2, we can see that a mean free path length of $< l >= 400$ μm already provides a noticeable change in the scattering phase function. The number of impurities per crystal which is required to obtain this value are approximately 6000, 700, and 4000 for $(NH_4)_2SO_4$ particles, air bubbles, and soot particles, respectively. Note that these numbers depend strongly on both the choice of the size distributions of the inclusions (see (6) and Table 1) and on the choice of the ice crystal size. Therefore they can only be regarded as a rough estimate of the order of magnitude of the required number of internal scatterers. Consequently, we limit our conclusions to the statement that it requires approximately 10^3 to 10^4 inclusions per ice crystal in order to get a noticeable change in its scattering features.

Table 2 lists the changes in the asymmetry parameter g and single-scattering albedo ω_0 of the crystal size distribution as a function of the internal mean free path length. Changes in ω_0 are shown for soot only since ammonium sulfate and air bubbles add no additional absorption to the ice particle. If the ice crystal itself is absorbing, even nonabsorbing contaminations would affect the overall absorption since they would change the photons path lengths inside the crystal. For the nonabsorbing inclusions, g decreases with increasing τ, whereas g increases with growing soot contamination. Again, this opposite behavior is due to the additional absorption at the soot particles, which lets the strongly forward scattering diffraction pattern more and more dominate the overall scattering features as the soot concentration increases. The decrease in g is stronger for ammonium sulfate than for air bubbles since the first one exhibits a more isotropic scattering characteristic. For $< l >= 400$ μm, g reduces by 0.004 (0.009) for ammonium sulfate (air bubble) inclusions. The asymmetry parameter increases by 0.022 for the soot-contaminated ice crystals. Thus soot provides the strongest absolute change in g. Note that soot is basically affecting the crystal scattering properties through the additional absorption, which is shown in the considerable reduction of the single-scattering albedo. A 10 times smaller soot contamination, i.e., $< l >= 4000\mu$m or 400 soot particles per crystal, results in a single-scattering albedo of 0.9991. Depending on the cloud optical thickness, this deviation from perfectly conservative scattering may have a noticeable impact of the clouds overall scattering and absorption properties.

Table 2. Asymmetry Parameter g of an Ice Crystal Containing Ammonium Sulfate, Air Bubble, and Soot Inclusions as a Function of Mean Free Path Length $< l >$

$l[\mu m]$	$g, (NH_4)_2SO_4$	g, Air Bubbles
∞	0.8153	0.8153
400	0.8113 (0.8370)	0.8060 (0.8340)
80	0.7841 (0.8832)	0.7722 (0.8740)
40	0.7588 (0.9079)	0.7385 (0.8953)
20	0.7215 (0.9284)	0.6935 (0.9131)
$l[\mu m]$	g, Soot	ω_0, Soot
∞	0.8153	1.0000
400	0.8372 (0.8484)	0.9249 (0.9307)
80	0.8905 (0.9253)	0.7128 (0.7372)
40	0.9233 (0.9686)	0.5906 (0.6125)
20	0.9512 (0.9945)	0.5164 (0.5253)

The changes in the single-scattering albedo ω_0 for crystals with (absorbing) soot inclusions are also shown. Results based on the independent scattering approximation are given in paranthesis.

4.2. Single-Scattering Simulations With an Independent Scattering Approximation

From a theoretical and practical point of view, it is interesting to compare the above discussed results with those obtained by an independent scattering approximation (ISA), where the scattering properties of ice and inclusions are treated separately, i.e., where radiative interactions between the ice particle and the embedded inclusions are neglected.

Since the internal scatterers do not affect the diffraction pattern of the ice crystal, the combination of the scattering phase functions of ice and inclusions reads

$$P_{\text{ref}}^{\text{ice+incl}} = \frac{\sigma^{\text{ice}} P_{\text{ref}}^{\text{ice}} + N^{\text{incl}} \sigma^{\text{incl}} P^{\text{incl}}}{\sigma^{\text{ice}} + N^{\text{incl}} \sigma^{\text{incl}}}, \qquad (7)$$

where $P_{\text{ref}}^{\text{ice}}$ denotes the reflection/refraction part of the ice crystal phase function; σ^{ice} and $N^{\text{incl}}\sigma^{\text{incl}}$ are the cross sections of the ice crystal and the N^{incl} internal scatterers; σ^{ice} equals the geometrical cross section of the ice crystal, i.e., one forth its surface area, while $N^{\text{incl}}\sigma^{\text{incl}} = V^{\text{ice}}/ < l >$, where V^{ice} is the volume of the ice crystal. The last expression results from (6).

The ray-tracing part of the single-scattering albedo can be written as $\omega_{0rt} = 2\omega_0 - 1$, where ω_0 denotes the total single-scattering albedo. This expression considers the nonabsorbing behavior of diffraction. In the case of internal absorbing scatterers, we have

$$\omega_{0\text{rt}} \leftarrow \omega_{0\text{rt}} \cdot (\omega_0^{\text{incl}})^{\frac{H}{<l>}}, \qquad (8)$$

where ω_0^{incl} denotes the single-scattering albedo of the internal scatterer (see Table 1). The exponent $H/ < l >$ corresponds to the average number of effective internal scattering events. The new total single-scattering albedo, including absorption at the ice crystal and at the internal scatterers, is then given by

$$\omega_0^{\text{ice+incl}} = \frac{1}{2}(1 + (2\omega_0 - 1)(\omega_0^{\text{incl}})^{\frac{H}{<l>}}) \qquad (9)$$

Substituting the results of (7) and (9) in (4) provides the total phase function of the independently treated ice crystal/inclusions combination. The corresponding asymmetry parameter and single-scattering albedos (for soot only) are compared to the results based on the RT/MC technique in Table 2, where ISA results are given in parantheses.

Obviously, the ISA does not give a satisfying estimate of the true scattering behavior, even for large internal path lengths, i.e., small number densities of the internal scatterers. For the nonabsorbing inclusions, g increases with decreasing $< l >$, contrary to the previous results. An independent superposition of the phase functions of ice crystal and inclusions basically affects the forward scattering region, side and backscattering is little influenced since both constituents are already predominantly forward scattering. As a result, the combined forward scattering behavior becomes broader, side and backscattering remains almost the same, and the asymmetry parameter increases. On the other hand, a change in the internal ray paths as simulated in the MC procedure not only influences the forward scattering behavior, but also all subsequent internal reflection events, leading to both a broadening of the forward scattering and a systematic increase in the side and backscattering. In other words, the scattering by the ice crystals and the internal inclusions are strongly coupled owing to the potential of the inclusions to systematically change the internal ray paths. In the case of absorption, either by the ice crystal or by the inclusions, the length of the effective ray paths and thus the coupling decreases. This is demonstrated by the soot inclusions, where MC/RT and ISA results agree better than for the nonabsorbing inclusions.

4.3. Multiple Scattering

In order to demonstrate the influence of ice crystal inclusions on the radiative properties of cirrus clouds, we performed Monte Carlo radiative transfer calculations with the above discussed single scattering phase functions and single-scattering albedos serving as input parameters. The Monte Carlo model is basically identical to the one used for the internal scattering events, except for the fact that the scattering medium is plane-parallel now.

Figure 3 shows the spherical reflectivity or spherical albedo R and spherical diffuse transmissivity T, as well as spherical absorptivity A, as a function of cloud optical thickness. The term "spherical" denotes the integration over all solar zenith angles [e.g., *Hansen and Travis*, 1974].

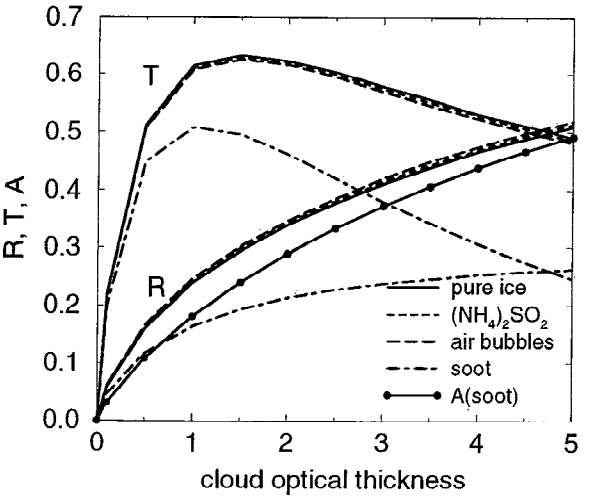

Figure 3. Spherical reflectivity R, diffuse transmissivity T, and absorptivity A of a homogenous, plane-parallel cirrus cloud as a function of cloud optical thickness and type of ice particle inclusions, i.e., ammonium sulfate, air bubbles, and soot. The inclusion number density inside the crystal is defined by $< l >= 400$ μm.

Because of energy conservation, we have $R + T + T_{\text{dir}} + A = 1$, where T_{dir} denotes the direct transmissivity. T_{dir} depends on cloud optical thickness only and is not discussed here. Results are shown for a monodisperse cloud. Only the one hexagonal ice crystal discussed above is considered. Furthermore, we limit our study to the $< l >= 400$ μm case, i.e., the smallest contamination density considered in this paper. Figure 3 shows that the nonabsorbing ammonium sulfate and air bubble inclusions provide only little changes in R and T compared to the pure ice crystal case. Both show a small increase in albedo and a decrease in diffuse transmissivity, caused by the slightly more isotropic single-scattering properties of the contaminated ice crystals. Soot inclusions, on the other hand, provide a strong change in the reflection and transmission features. R and T are considerably attenuated, first of all, due to the additional cloud absorption and, to a smaller extent, due to the less isotropic scattering behavior of the "soot crystals", respectively.

5. Conclusions

The demonstrated influence of different types of inclusions on the single- and multiple-scattering behavior of hexagonal ice crystals may serve as an additional motivation for studying the microphysical properties of ice crystals, including their internal structure. A better estimate of the discussed impurity effects requires a more precise knowledge of realistic number densities of inclusions. Since these impurities behave differently from distortions of particle shapes, our qualitative results hold for particle shapes other than hexagonal columns as well.

A noticeable change in both single- and multiple-scattering properties requires approximately 10^3 to 10^4 inclusions per ice crystal. Neglecting the magnitude of this number, we may conclude that soot contamination clearly provides the strongest effect on the ice crystal and cirrus cloud radiative properties. This effect basically results from the additional absorption at the internal soot scatterers. Thus, from the radiative transfer standpoint, it is most interesting to obtain some reliable numbers of absorbing ice crystal inclusions inside natural and man-made ice clouds.

There is some experimental evidence that soot contaminations are more likely to be found at the outer boundaries of the ice particles (J. Hallet, private communication, 1995) in which case the model presented here requires some substantial changes regarding the treatment of reflection and refraction processes. Furthermore, a large number of air bubbles may be found in suddenly frozen, supercooled droplets (Hallet, private communication, 1995) which motivates the treatment of spherical rather than hexagonal crystal geometries.

Finally, ice inclusions are not necessarily spherical in shape, which may prevent the use of Mie theory to solve their single-scattering properties. Additional work may take advantage of results from scattering theories like the T-matrix method [*Mishchenko,* 1993] or the discrete dipole approximation [*Draine and Flatau,* 1994], which are suitable for non-spherical particle shapes.

Acknowledgments. We are gratefull to Barbara Carlson, Andy Lacis, and Ina Tegen for helpful discussions. This work was supported by the NASA FIRE III Project.

References

Draine, B. T., and P. J. Flatau, Discrete-dipole approximation for scattering calculations, *J. Opt. Soc. Am. A, 11*, 1491–1499, 1994.

Hansen, J. E., and L. D. Travis, Light scattering in planetary atmospheres, *Space Sci. Rev., 16*, 527–610, 1974.

Heymsfield, A. J., K. M. Miller, and J. D. Spinhirne, The 27-28 october 1988 fire cirrus case study: Cloud microstructure, *Mon. Wea. Rev., 118*, 2313–2328, 1990.

Jensen, E. J., and O. B. Toon, Ice nucleation in the upper troposphere: Sensitivity to aerosol composition and size distribution, temperature and cooling rate, *Geophys. Res. Lett., 21*, 2019–2022, 1994.

Macke, A., Scattering of light by polyhedral ice crystals, *Appl. Opt., 32*, 2780–2788, 1993.

Macke, A., J. Mueller, and E. Raschke, Single scattering properties of atmospheric ice crystals, *J. Atmos. Sci, 53*, 2813–2825, 1996.

Mishchenko, M. I., Light scattering by size-shape distribution of randomly oriented axially symmetric particles of a size comparable to a wavelength, *Appl. Opt., 32*, 4652–4666, 1993.

Mishchenko, M. I., D. W. Mackowski, and L. D. Travis, Scattering of light by bispheres with touching and seperated components, *Appl. Opt., 34*, 4589–4599, 1995.

Mitchell, D. L., and W. P. Arnott, A model predicting the evolution of ice particle size spectra and radiative properties of cirrus clouds. Part II: Dependence of absorption and extinction on ice crystal morphology, *J. Atmos. Sci, 51*, 817–832, 1994.

Nilsson, B., Meteorological influence on aerosol extinction in the 0.2 - 40 μm wavelength range, *Appl. Opt., 18*, 3457–3473, 1979.

Raes, F., J. Wilson, and R. Van Dingenen, Aerosol dynamics and its implications for the global aerosol climatology, in *Aerosol forcing of climate*, edited by R. Charlson, and J. Heintzenberg, 153–169, John Wiley & Sons, 1995.

Sassen, K., O. D. Starr, G. G. Mace, M. R. Poellot, S. H. Melpi, W. L. Eberhard, J. D. Spinhirne, E. W. Eloranta, D. E. Hagen, and J. Hallet, The 5-6 december 1991 FIRE IFO II jet stream cirrus case study: Possible influence of volcanic aerosols, *J. Atmos. Sci, 52*, 97–123, 1995.

Schumann, U., On the effect of emissions from aircraft engines on the state of the atmosphere, *Ann. Geophysicae, 12*, 365–384, 1994.

Takano, Y., and K. N. Liou, Radiative transfer in cirrus clouds. Part III: Light scattering by irregular ice crystals, *J. Atmos. Sci, 52*, 818–837, 1995.

Toon, O. B., J. B. Pollack, and B. N. Khare, The optical constants of several atmospheric aerosol species: Ammonium sulfate, aluminium oxide, and sodium chloride, *J. Geophys. Res., 81*, 5733–5748, 1976.

Warren, S. G., Optical constants of ice from the ultraviolet to the microwave, *Appl. Opt., 23*, 1206–1225, 1984.

Brian Cairns, Andreas Macke (corresponding author), and Michael I. Mishchenko, Goddard Institute for Space Studies, 2880 Broadway, New York, NY 10025. (e-mail: brian@memphis.giss.nasa.gov and amacke@giss.nasa.gov and crmim@giss.nasa.gov)

(Received December 6, 1995; revised June 28, 1996; accepted July 12, 1996.)